

# Ribo-ODDR: Ribo-seq focused Oligo Design pipeline for experiment-specific Depletion of Ribosomal RNAs

Ferhat Alkan<sup>1,\*</sup>, Joana Silva<sup>1</sup>, Eric Pintó Barberà<sup>1</sup>, William J. Faller<sup>1,†</sup>

<sup>1</sup>Division of Oncogenomics, The Netherlands Cancer Institute, Plesmanlaan 121, 1066 CX, Amsterdam, The Netherlands

## Abstract

Ribosome profiling (Ribo-seq) has revolutionized the study of RNA translation. The technique provides information on ribosome positions across all translated RNAs with nucleotide-resolution. However, several technical limitations restrict the sequencing depth of such experiments, the most common of which is the overabundance of ribosomal RNA (rRNA) fragments. Various strategies have been employed to tackle this issue, including the use of commercial rRNA depletion kits, however these may perform suboptimally. Here we show that the rRNA fragments generated via Ribo-seq vary significantly with differing experimental conditions, suggesting that a “one-size-fits-all” approach may result in inefficient rRNA depletion. In order to overcome this it is possible to use custom-designed biotinylated oligos complementary to the most abundant rRNA fragments, however currently no computational framework exists to aid the design of optimal oligos. We have developed *Ribo-ODDR*, an oligo design pipeline integrated with a user-friendly interface that assists in oligo selection for efficient experiment-specific rRNA depletion. *Ribo-ODDR* uses preliminary data to identify the most abundant rRNA fragments, and calculates the rRNA depletion efficiency of potential oligos. We show that *Ribo-ODDR* designed oligos lead to a significant increase in rRNA depletion, and increased sequencing depth as a result. *Ribo-ODDR* is freely accessible at <https://github.com/fallerlab/Ribo-ODDR>

## 1 Introduction

Since its development, Ribosome Profiling (also known as Ribo-seq) has revolutionized the study of RNA translation [1]. The technique allows the analysis of ribosomally associated mRNA at codon-level resolution, providing a snapshot of the mRNAs bound by ribosomes in the cell. Information on translation efficiencies, open reading frame (ORF) usage, translation start sites, ribosome pause sites, amino acid dependencies, and translation elongation rates can be gleaned from the data generated (reviewed in [2]). Additionally, the level of ribosome binding to an mRNA is a much better predictor of protein levels than the quantity of mRNA that is present, underscoring the importance of this technique [1, 3].

The Ribo-seq protocol takes advantage of the fact that at any instant a ribosome covers a ~28 nucleotide fragment of mRNA. This fragment is protected from nuclease digestion as a result and is hence known as the ribosome protected fragment (RPF). Following ribosome stalling with translation blockers (i.e. cycloheximide), isolation of a cell lysate, and treatment with RNase, a cDNA library can be made from the resulting RPFs, and sequenced. By selecting the correct fragment size, the abundance of ribosomes at every location on the transcriptome can be deduced.

Although this process has been somewhat standardized [4], it is acknowledged that numerous problems remain in generating high quality data. The RNase enzyme used [5], or length of digestion [6] can significantly bias the resulting data. Additionally, it is a common problem that a high proportion of sequencing reads derive from rRNA sequences, despite the use of rRNA depletion strategies. Indeed, in most experi-

\*Software-related correspondence should be addressed to f.alkan@nki.nl

†Corresponding Author, email: w.faller@nki.nl

ments rRNA make up between 30 and 70% of all reads sequenced [4], and more than 90% in some cases [7].

At present, the most common rRNA depletion strategies include the use of commercial rRNA depletion kits or the use of custom-designed biotinylated oligos previously reported in the literature. Both of these approaches make use of RNA oligos that are complementary or near-complementary to the rRNA, thus binding to their target rRNA sequence and allowing their depletion with a simple fishing approach. Additionally, the use of duplex-specific nuclease (DSN) has been reported [8]. However, DSN is known to also deplete highly expressed genes, and both commercial kits and custom oligos assume that the rRNA fragments present in a sample are consistent across experiments. Here we show that this is not the case, and that the experimental conditions and the tissue being used both introduce variations in the abundance of rRNA fragments produced. This raises the possibility that differential efficiencies of rRNA depletion across samples in an experiment may introduce biases in Ribo-seq data.

There are a number of possible approaches that could be taken to circumvent this problem. For example, there may be previously published data that provides a list of oligos that is confirmed to be efficient for Ribo-seq performed in a specific tissue and organism, following a specific protocol. However these pre-designed oligos may need further optimization. For example, the overall efficiency of pre-designed oligos can be improved by their cross-species optimization. Oligos designed for any source organism can be transferred to a target organism by identifying which regions are targeted in the source and designing new perfect-complementary oligos for the positional equivalent region in the target organism.

The most reliable way to confront the problem of differential rRNA fragmentation is to perform pilot experiments on identical or similar samples and design novel biotinylated oligos that targets the most abundant rRNA fragments within generated pilot data [9]. Unfortunately, this approach requires experimental effort and computational work, potentially with a few rounds of optimization. However, this could be avoided

due to the increasing number of Ribo-seq datasets from diverse sources that are being published, which could also serve as pilot data for researchers. Using this data, the most abundant rRNA fragments can be identified, and oligos designed to deplete them.

With this study, we first provide evidence that commercial rRNA depletion kits perform suboptimally and rRNA fragments generated by nuclease treatment differ substantially under various experimental conditions. Furthermore, we show that the same variability exists in fragments generated from different organs, even when using identical protocols. To tackle this problem, we present *Ribo-ODDR*, a Ribo-seq focused Oligo Design pipeline for Depleting rRNAs. This pipeline addresses and automates the above mentioned problems and allows the design or optimization of oligos with high rRNA depleting potential, based on preliminary or previously published data. It is freely accessible through GitHub in order to help researchers improve the power of their Ribo-seq experiments through more efficient rRNA depletion, thus maximizing the information gained from Ribo-seq experiments.

## 2 MATERIALS AND METHODS

We first introduce the public datasets that are actively analyzed in this study to show the suboptimal performance of commercial rRNA depletion kits and rRNA fragment differences within different Ribo-seq experiments performed in the same species. Our analyses with these datasets serve as a justification for the experiment-specific depletion of rRNAs with custom oligos. Then, we describe the details of the *Ribo-ODDR* oligo-design pipeline and present its different modes of action. Finally, we explain the followed Ribo-seq protocol for the experiments performed within this study.

### 2.1 Ribo-seq with commercial rRNA depletion kit

Suboptimal performance of commercial rRNA depletion kits in Ribo-seq experiments is a known issue [8] and we provide evidence on this by analysing two public datasets [10, 8]. First study [10] uses the Ribo-Zero Gold rRNA Removal Kit (H/M/R) (Illumina, catalog no. MRZG126), whereas the second [8]

uses a different version (Human/Mouse/Rat: Epicentre, cat. no. RZH1046, Plant Seed/root: Epicentre, cat. no. MRZSR116). We accessed this data through NCBI using GSE96998 and SRP102438 accession IDs for the former, and through ENA using ERR894498 accession ID for the latter. Upon downloading the raw fastq files, we trimmed the adapters and cleaned the size selection markers using the cutadapt tool [11]. The rRNA fragments were then identified through mapping the trimmed read files to mouse 28S (NR\_003279.1), 18S (NR\_003278.3), 5.8S (NR\_003280.2) and 5S (NR\_030686.1) rRNA sequences, using the TopHat aligner [12]. We also mapped them to mouse protein-coding transcript sequences (gencode release M21) after cleaning rRNA fragments using the *SortMeRNA* tool [13], and calculated the rRNA percentages in the samples by dividing the number of rRNA-mapping reads by the total number of reads that maps to rRNAs or protein coding transcripts.

## 2.2 Organ-specific *in vivo* Ribo-seq dataset

To provide evidence on the necessity of experiment-specific rRNA depletion, we made use of a comprehensive public dataset that generated *in vivo* Ribo-seq data for multiple tissues in mouse [14]. This dataset includes 9 organs (brain, heart, kidney, liver, lung, pancreas, skeletal muscle, spleen and testis) where experiments are performed in replicates for each organ. The study measures the translation elongation rate differences between different mouse organs with time-course experiments using both harringtonine and cycloheximide. In our analysis we only used samples treated with cycloheximide. One should note that no rRNA depletion protocol was applied within included experiments, however, RNA digestion was performed differently for two groups of samples. For pancreas, spleen and lung, only RNaseT1 nuclease was used for digestion, but for the others, a fixed mix of RNaseT1 and RNaseS7 nucleases was used. This difference enables us to analyze not only the tissue specificity of rRNA fragments but also their technical dependency on the used experimental protocol. Raw sequencing data (fastq files) of this dataset were first downloaded through NCBI with GSE112223 and SRP136268 accession IDs, then, raw reads were trimmed using the cutadapt tool [11] before running the *Ribo-ODDR*

pipeline (*design-mode*) with generated trimmed read files.

## 2.3 The *Ribo-ODDR* pipeline

The primary aim of the *Ribo-ODDR* pipeline is to aid the biotinylated oligo design process for the depletion of rRNA fragments in Ribo-seq experiments. This includes designing novel oligos based on pilot experimental data and cross-species optimization of pre-compiled oligo sets. The *Ribo-ODDR* software comes as an executable Python3 script and has a flexible design for different user needs. It does not contain any compiled information on rRNA sequences, enabling *Ribo-ODDR* to be applied on an organism of choice as long as rRNA (or other depletion-intended RNA) sequences are provided by the user.

In the subsections below, we first describe how *Ribo-ODDR* performs the cross-species optimization of pre-compiled oligo sets in its *cross-species optimization mode*. Then, we continue with the details of the used methodology, when designing novel oligos based on the pilot experimental data in the *novel oligo design mode*. Designed oligos, regardless of the *Ribo-ODDR* mode used, are reported to the user in *FASTA*, *CSV*, *BED* and *GFF3* file formats. These files contain various relevant information on oligo designs, including depleting potential (percentage of rRNA fragments that can be depleted with that oligo) in pilot samples, positions of the targeted rRNA regions, GC contents, hybridization energies and oligo self-folding statistics. One should also note that, in the *novel oligo design mode*, *Ribo-ODDR* does not provide a final optimal set of oligos to deplete rRNA fragments. Instead, it reports the depleting potential of all high potential oligos to the user together with other information on these designs. This is in parallel with our flexible software approach. However, *Ribo-ODDR* provides a ‘*Ribo-ODDR oligo-selector*’ user interface to aid the oligo selection process. This interface is presented in the last subsection below. The full workflow of the *Ribo-ODDR* (*novel oligo design mode*) is shown in Figure 1.

### 2.3.1 Cross-species optimization mode

In this mode, *Ribo-ODDR* requires users to provide the sequences of the precompiled oligo set (designed for

## Pilot Experiments

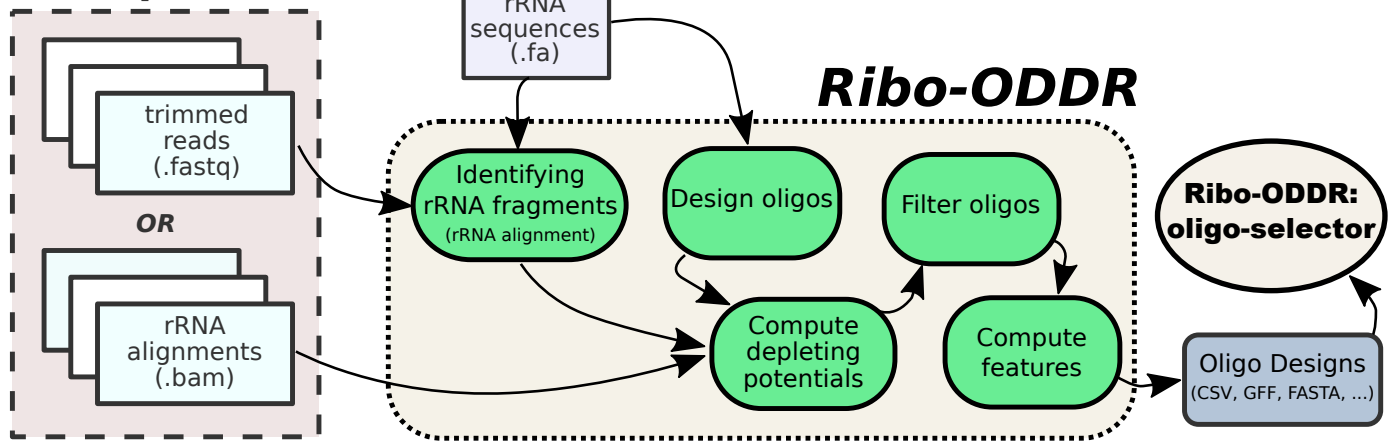


Figure 1: The workflow diagram for the *Ribo-ODDR* pipeline (*novel oligo design mode*).

source organism rRNAs) and target rRNA sequences for the organism to perform Ribo-seq in. Due to the complexity of determining functional homology of rRNA regions between source and target rRNA sequences, we follow a different approach for cross-species optimization. Using *RISearch2* RNA-RNA interaction prediction tool [15], *Ribo-ODDR* first identifies the most likely target regions of source oligos in the target, accepting the interaction with lowest hybridization energy as most probable. Then, for each source oligo, *Ribo-ODDR* designs the new oligo as perfect complementary to the target interaction region. To reach equivalent coverage as the source oligo, target oligo is later extended on both ends according to oligo dangling ends within the source oligo-target rRNA interaction structure (extending by one for each unpaired nucleotide on 5' and 3' ends of the oligo). Note that in the presence of high sequence homology between source and target rRNA sequences, *Ribo-ODDR* can report the same source oligos as optimized oligos.

### 2.3.2 Novel oligo design mode

The aim of this mode is to compute the depleting potential of all novel oligos on the given pilot Ribo-seq data. In a simple use-case, it requires user to provide the rRNA sequences, the length range of desired oligos, and the pilot data in which rRNA fragments are abundant. First step of the mode is the identification of rRNA fragments through aligning Ribo-seq reads to user-given rRNA sequences. Next, information on

these fragments are used to calculate the depleting potential of all potential oligos that satisfies the user-given length range. Later, *Ribo-ODDR* outputs this information together with various statistics on the designed oligos and final selection of oligos is done by the user using '*Ribo-ODDR oligo-selector*', a user-friendly straightforward R-Shiny user interface.

**Identifying rRNA fragments:** Several variations of the Ribo-seq protocol exist, and for most the generated sequencing data requires trimming of adapter sequences and/or cleaning of used size selection markers before aligning to genome or transcriptome. *Ribo-ODDR* does not perform these pre-processings itself, therefore, requires user to preprocess the sequencing data prior to *Ribo-ODDR*. Under default settings, trimmed & cleaned reads, provided as input pilot data by the user, are first aligned to rRNA sequences using the TopHat aligner [12]. This is done with the following parameter settings, `-n 2 -no-novel-juncs --no-novel-indels --no-coverage-search --segment-length 25`. However, users can also perform this alignment using other read-aligners and provide the generated bam files as input to *Ribo-ODDR*.

**Oligo-set generation and depleting potential computation:** Next, based on the user-given oligo length range constraint, depletion oligos are generated in a position specific manner. Oligo designs correspond to fixed length regions within user-given rRNA sequences, an oligo sequence being the perfect complementary sequence to its region. Note that the fi-

nal oligo-set spans all possible regions across all given rRNA sequences. Therefore, oligo designs overlap with each other but the depleting potential of each oligo is computed separately. Following a heuristic approach, *Ribo-ODDR* computes the depleting potential of an oligo (separately for each pilot sample) based on the number of depletable rRNA fragments, i. e. reads that are aligned to the corresponding oligo region within an rRNA. To allow sub-optimal binding between rRNA fragments and the oligo, a fragment (read) is considered depletable only if it satisfies the following constraints. The rRNA fragment has to cover minimum of 10 nucleotides or two thirds of the oligo length, whichever is higher, within the oligo region under consideration. Additionally, the rRNA fragment can have a maximum of 10 nucleotides or one third of the oligo length, whichever is lower, outside the oligo region to be considered as depletable by that oligo. Based on these constraints, for each pilot sample, we simply count the number of depletable fragments for every oligo and report its percentage within all rRNA fragments as the depleting potential for each pilot sample.

#### Filtering oligos based on depleting potential:

For fast computation of oligo features, *Ribo-ODDR* filters out some of the low potential oligos based on customizable thresholds. Under default settings, it discards the oligos that have a depleting potential less than 0.05 (5% of all rRNA fragments) in more than 75% of the provided pilot samples. However, these thresholds can be altered by the user.

**Computation of other oligo features:** In addition to sample-specific depleting potential of oligos in pilot samples, *Ribo-ODDR* reports a few other informative statistics on designed oligos, for which some are straightforward like *GC\_content* and *target\_rRNA\_position*. For each oligo, an *overall\_depletion\_score* is also computed by *Ribo-ODDR*, that is the ratio of samples oligo has a depleting potential more than a user-given threshold, 0.05 (5%) in default settings. Additionally, for each oligo, *Ribo-ODDR* reports a *minimum\_hybridization\_energy* that is the free energy of the full perfect complementary binding to an rRNA fragment at 37°C computed by *RIsrch2* [15]. Using the *RNAfold* program from the ViennaRNA Package [16], self-folding of the oligo is also predicted. This is reported in three different features, predicted *structure*, the *MFE*

as the free energy of the predicted structure, and the *base\_pairing\_percentage* within the given structure.

**Off-target prediction for designed oligos:** If protein-coding transcript sequences of the organism are provided by the user, *Ribo-ODDR* computes the off-targeting potential of oligos as well. Denoting the minimum binding free energy across all oligos as  $E_{min}$  and the minimum oligo length as  $l_{min}$ , oligo off-targets are predicted using *RIsrch2* [15] with the following parameter settings,  $-s l'_{min} -e E'_{min}$ , where  $l'_{min} = \lfloor 0.75 \times l_{min} \rfloor$  and  $E'_{min} = \min(-25, 0.5 \times E_{min})$ . These settings allow us to detect the potential off-target regions on given transcripts, that has a considerably low binding energy with designed oligos. Number of predicted off-targets are reported to the user as an additional oligo feature, however, the additional information on individual off-target predictions are outputted separately.

### 2.3.3 Selecting final oligos with *Ribo-ODDR* oligo-selector:

To aid the final selection of oligos from all oligos outputted by the *Ribo-ODDR* novel oligo design mode, we present the *Ribo-ODDR* oligo-selector auser interface, that uses the R-shiny environment. In this interface, users can explore the features of the designed oligos within the available-oligo-list, filter them according to different filters on reported features and add the desired ones to the selection list, which results in removing the overlapping oligos from the available oligo list. A snapshot from this interface is shown in Supplementary Figure 1.

## 2.4 Experimental details on Ribo-seq experiments

*C57BL/6* female and male mice between 8 and 12 weeks of age were used for experiments. Both *Lgr5Cre<sup>ERT2</sup>* [17] and *VillinCre<sup>ERT2</sup>* [18] mice were crossed to the RiboTag mouse [19] to generate *Lgr5Cre<sup>ERT2</sup>RPL22.HA* and *VillinCre<sup>ERT2</sup>RPL22.HA* respectively. Due to differences in recombination efficiency and total number of cells, the tamoxifen-mediated induction of Cre-recombinase varied slightly between the two lines: for the *Lgr5Cre<sup>ERT2</sup>RPL22.HA* mice, recombination was induced by a single intraperitoneal injection of 120 mg/kg tamoxifen and samples

were taken for downstream analysis after 24h and 48h; for the *VillinCreERT2RPL22.HA* mice, recombination was induced after two consecutive intraperitoneal injections of 80 mg/kg tamoxifen and samples were taken after 120h. Mice were bred in-house at the Netherlands Cancer Institute and all experimental protocols were approved by the NKI Animal Welfare Body.

#### 2.4.1 Sample preparation from *in vivo* small intestines:

Mice were euthanized by CO<sub>2</sub> and small intestines were immediately dissected, flushed with cold PBS supplemented with 100 µg/mL of cycloheximide and snap frozen using liquid nitrogen. Frozen tissues were ground by pestle and mortar while submerged in liquid nitrogen. The resulting powder was rapidly dissolved in cold lysis buffer (20 mM Tris HCl pH 7.4, 10 mM MgCl<sub>2</sub>, 150 mM KCl, 1% NP-40, 100 µg/mL cycloheximide and 1x EDTA-free proteinase inhibitor cocktail (Roche, 04693132001)) and incubated on ice for 30min. Samples were then homogenized using a Tissue Lyser (3 rounds of 45 sec at 50 oscillations per second) and centrifuged at max speed for 20min at 4 °C.

#### 2.4.2 Sample preparation from *in vitro* crypt cultures:

Crypt cultures were generated from the *VillinCreERT2RPL22.HA* mice as described previously [20]. Around 120 plugs of 30 µL BME (Amsbio #3533-010-02) were used for each sample. Ribosomes were stalled by incubating cells with 100 µg/mL cycloheximide for 3-5min at 37 °C, after which all steps were carried on ice. Cells were collected and washed twice in cold PBS supplemented with 100 µg/mL cycloheximide, and homogenized with a 25G needle in cold lysis buffer. After incubating the lysates on ice for 20min, samples were centrifuged at max speed for 20min at 4 °C.

#### 2.4.3 Ribosome profiling

**Pull down of HA-tag ribosomes:** All supernatants (from both *in vivo* small intestines and *in vitro* crypt cultures) were pre-cleared for 20min at 4 °C, using Pierce™ Control Agarose Matrix (ThermoFisher #26150), after which they were incubated

with pre-washed Anti-HA.11 Epitope Tag Affinity Matrix (BioLegend #900801) overnight at 4 °C. Ribosomes were eluted in lysis buffer containing 200 µg/mL HA peptide (ThermoFisher #26184) and supplemented with 100 µg/mL cycloheximide for 15min at 30 °C. Exposed RNA was digested with RNase I (ThermoFisher #AM2294) for 40min at 25 °C and this process was stopped by adding SUPERASE (ThermoFisher #AM2694). RPFs were purified using the miRNeasy minikit (Qiagen #217004) following the manufacturer's protocol and used for the library preparation.

**Library preparation:** The library preparation was conducted as previously described [21] with some modifications. Briefly, RPFs were run in a 10% TBE-Urea polyacrylamide gel and size selected between 19 nt and 32 nt as marked by RNA oligonucleotides (see Supplementary Table 1). Gel slices were crushed, eluted and ethanol precipitated. Samples were then dephosphorylated in the 3' region using T4 polynucleotide kinase (PNK) (NEB #M0201) and 1.5xMES buffer (150 mM MES-NaOH, 15 mM MgCl<sub>2</sub>, 15 mM β-mercaptoethanol and 450 mM NaCl, pH 5.5) and incubated at 37 °C for 4h. RNAs were purified using Trizol and the 3' adapter (see Supplementary Table 1) was added using T4 RNA ligase I (NEB #M0204) at 24 °C overnight. The ligated products were size selected and 5' phosphorylated with T4 PNK for 30min at 37 °C. After purifying the RNAs, the 5' adaptor (see Supplementary Table 1) was added with T4 RNA ligase I for 2,5h at 37 °C and the final products with both adaptors were size selected one last time on a 10% TBE-Urea polyacrylamide gel. To deplete rRNAs, samples were incubated with 2 µL of the different biotinylated oligos (10 µM each oligo, Supplementary Table 2-4) in 20 µL with 2xSSC (ThermoFisher #15557044). Samples were then denatured at 100 °C for 1min, followed by an incubation at 37 °C for 15min. In the meantime, 40 µL of MyOne Streptavidin C1 DynaBeads (ThermoFisher #65001) were washed and re-suspended in 20 µL of 2x wash/bind buffer (2 M NaCl, 1 mM EDTA, 5 mM Tris and 0.2% Triton X-100) and mixed with the sample at 1000rpm for 30min and at 37 °C. Supernatants were collected and RNAs were precipitated with isopropanol and re-suspended in 8 µL of RNase-free water. Reverse transcription was performed with SuperScript III (ThermoFisher #18080051) following

the manufacturer’s instructions and using the RTP primer (see Supplementary Table 1). cDNA was then purified using G-50 columns (Merck GE27-5330-01) and used as a template for the PCR reaction with Phusion High-Fidelity DNA Polymerase (ThermoFisher #F530L) for 18 cycles, with primers listed in Supplementary Table 1. PCR products were purified using the QIAquick PCR purification kit (Qiagen #28104) followed by a E-Gel SizeSelect II 2%, (ThermoFisher #G661012). The quality and molarity of the samples were evaluated with the Agilent 2100 Bioanalyzer and the libraries were sequenced on the Illumina HiSeq2500 by the Genomics Core Facility at the Netherlands Cancer Institute.

**Data processing:** Raw reads are trimmed and cleaned from the size selection markers using the cutadapt tool [11]. Then, *Ribo-ODDR (design-mode)* is run with generated trimmed read files to align reads to mouse rRNA sequences (28S: NR\_003279.1, 18S: NR\_003278.3, 5.8S: NR\_003280.2, 5S: NR\_030686.1) and to design depletion oligos. To obtain the total number of reads mapped to protein coding transcripts, preprocessed reads are cleaned from rRNA fragments using the *SortMeRNA* tool [13] and remaining reads are mapped to gencode release M21 protein-coding transcript sequences using the TopHat aligner [12].

## 3 RESULTS

### 3.1 Suboptimal rRNA depletion of Ribo-Zero commercial kit

To test the efficiency of commercially available rRNA depletion products, we analyzed a previously published dataset that made use of the Ribo-Zero kit for Ribo-seq [10]. Surprisingly, analysis of this data showed that despite rRNA depletion, there was still a high abundance of rRNA fragments in both samples used in this experiment. Of all reads that could be mapped to rRNA and protein coding transcripts, 70% and 64% of them were rRNA fragments (Figure 2, upper 2 samples in both 28S rRNA and 18S rRNA). These unexpectedly high percentages significantly reduce the resolution of the performed experiments. Using the *svist4get* tool [22], we observed that rRNA depletion using this method resulted in the incomplete depletion of 28S and 18S rRNA fragments, particularly those originating

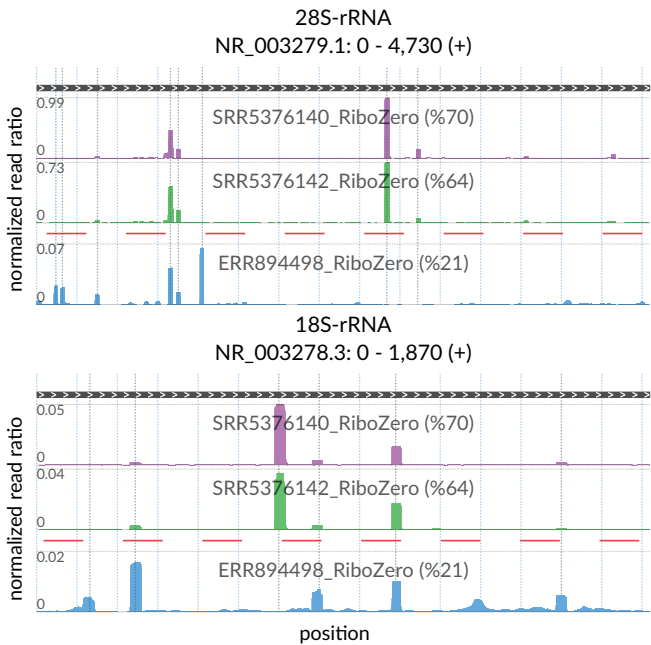


Figure 2: Suboptimal performance of the Ribo-Zero kit. Visualization is based on public Ribo-seq datasets where RiboZero kit was used for rRNA depletion. Each track shows the positional abundance profile of 28S (top) and 18S (bottom) rRNA fragments coming from individual samples. Red dashed line separates the datasets. For every position in the x-axis, y-axis represents the normalized read ratio, number of rRNA reads mapped to that position divided by the total number of reads mapped to all protein coding transcripts. Sample-specific total rRNA percentages are given in track labels together with SRA and ENA accession IDs for analyzed experiments.

from one rRNA hotspot within 28S. In both samples, this single undepleted fragment alone accounted for almost as many sequencing reads as all protein-coding transcript reads (see upper 2 samples in 28S rRNA in Figure 2). Several other fragments could also be found in relatively high abundance. The same analysis for 5-8S and 5S rRNAs can be found in the Supplementary Figure 2. Analysis of a second dataset that used the Ribo-Zero kit [8] also showed incomplete rRNA depletion. Interestingly however, while there was some overlap in the rRNA fragments that remained, the most abundant fragments were not shared between the experiments (Figure 2). These observations suggests that custom-designed rRNA depletion oligos are still

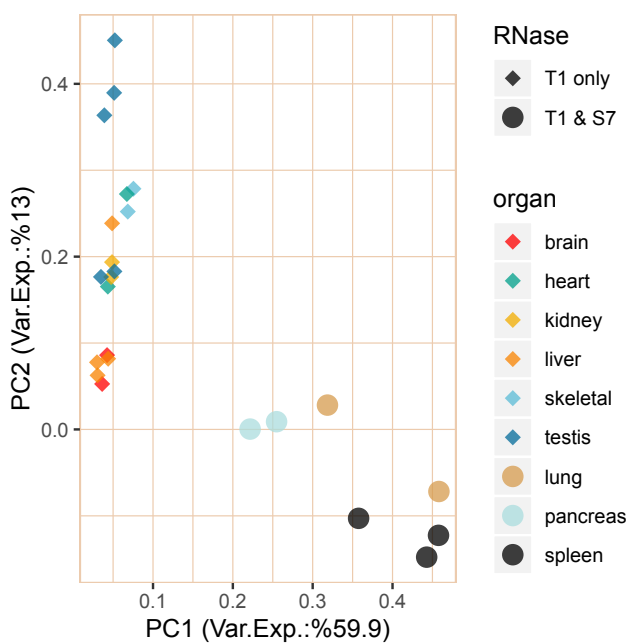


Figure 3: Principal component analysis (PCA) of rRNA fragment abundance profiles generated for all samples of the analyzed dataset. For every sample, positional abundance profile is created by counting the number of reads that map to every position on 28S, 18S, 5-8S and 5S rRNAs, and normalizing them by the total number of reads that map to protein-coding transcripts for that sample. PCA analysis is performed based on these profiles, with the first and second principal components plotted against each other, PC1 in x-axis and PC2 in y-axis. The percentage of variance explained by each component is given in corresponding axis labels.

advisable when using this commercial kit, in order to increase the overall resolution in Ribo-seq experiments.

### 3.2 Tissue and RNase specificity of rRNA fragments in mouse

The use of custom-designed biotinylated oligos serves as a good alternative to overcome the inefficiency of rRNA depletion in Ribo-seq experiments using commercial kits. However, there is no consensus on which oligos to use for maximal rRNA depletion, or even whether the same oligos would be suitable for different experiments. Our results above would suggest that this is not the case. Accordingly, we sought to mea-

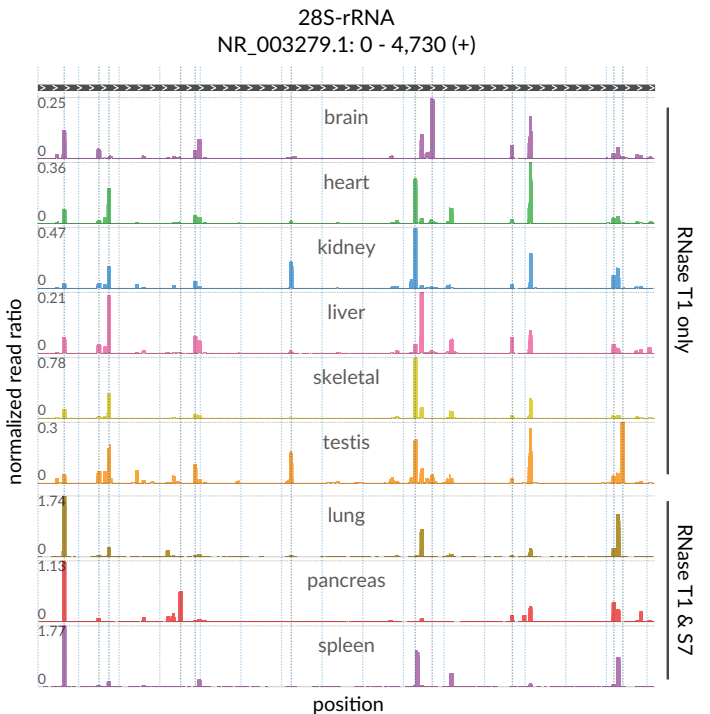


Figure 4: Tissue and RNase specificity of rRNA fragments in mouse. Each track shows the positional abundance profile of 28S rRNA fragments within the representative sample of the labeled organ. For every position in the x-axis, y-axis represents the normalized read ratio, number of rRNA reads mapped to that position divided by the total number of reads mapped to all protein coding transcripts.

sure the variability in rRNA fragment position and abundance in samples generated using slightly different protocols and tissues of origin. To do this, we made use of a previously published dataset in which the authors performed *in vivo* Ribo-seq in nine different mouse organs without any rRNA depletion protocol [14]. In this dataset, three sets of samples (lung, pancreas, and spleen) were digested using a mix of RNaseT1 and RNaseS7, with the remaining 6 (brain, heart, kidney, liver, skeletal muscle, and testis) being digested with only RNaseT1. After identifying 28S, 18S, 5-8S and 5S rRNA fragments separately for each sample, we compared their positional abundance profiles (based on number of fragments mapped to each position in rRNAs) with a principal component analysis (see Figure 3). This analysis revealed a striking heterogeneity in rRNA fragments in samples gener-

ated using different protocols, suggesting that efficient rRNA depletion oligos in one experiment may not be suitable for another. This protocol-derived heterogeneity of rRNA fragments can also be clearly observed in Figure 4, where the positional abundance profiles 28S rRNA fragments are shown for individual organs (one representative sample for each).

Moreover, the PCA analysis and abundance profiles also reveal significant rRNA fragment differences in samples generated from different organs using the same protocol. While our analyses showed that there is a strong agreement between replicate measures of each organ in terms of rRNA fragments produced (Figure 3 and Supplementary Figure 4-12), we observed clear profile separation between organs, particularly in those generated from the 28S rRNA (Figure 4). This is likely due to the shorter length of the 18S, 5-8S and 5S rRNAs, shown in Supplementary Figure 3. This suggests that rRNA fragment heterogeneity is a common occurrence, and clearly shows that a “one size fits all” approach is not appropriate in Ribo-seq experiments.

### 3.3 Comparing the depleting potential of oligos across different experiments

In order to understand the effect that this rRNA fragment heterogeneity has on the efficiency of rRNA depletion oligos, we developed *Ribo-ODDR*. Based on given pilot Ribo-seq data, this pipeline measures the depleting potential of all possible oligos. For each oligo, this potential is simply equal to the percentage of rRNA fragments produced from the oligo target region on the rRNA, where the oligo sequence binds with perfect complementarity (see Materials and Methods for a detailed description).

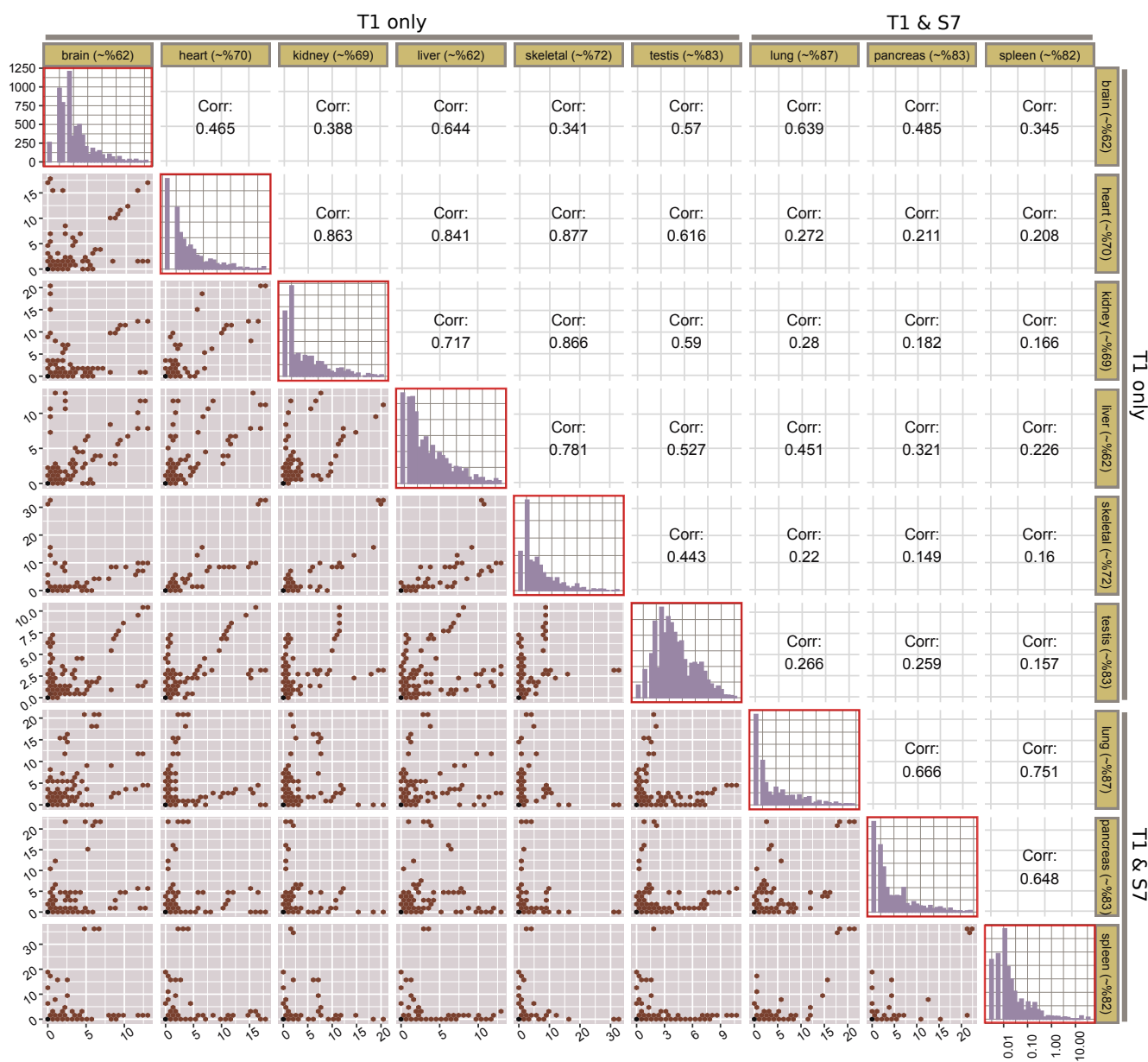
We ran *Ribo-ODDR* on the organ-specific data used above and obtained the sample-specific depleting potentials of all 25 nt long oligos ( $n = 6782$ ) that can deplete mouse 28S, 18S, 5-8S and 5S rRNA fragments. For each individual oligo, we also calculated the depleting potential within replicates of the same organ. Organ-specific depleting potential was calculated by simply averaging the values computed for each replicate of that organ.

In Figure 5, we compare the depleting potentials of oligos across all organ pairs with a cross-organ correlation analysis. This data makes it clear that the correlation in oligo depleting potential between sam-

ples treated using the same RNase digestion strategy is significantly higher than those using another strategy. For the RNaseT1/S7 digestion group, intra-group Pearson’s correlation coefficients are between 0.64 and 0.76 (mean value of 0.69), and for the RNaseT1-only group this is between 0.34 and 0.88 (mean value of 0.64). This confirms our observations detailed in Figure 4, demonstrating the influence of experimental conditions on the rRNA fragments created.

The cross-replicate correlation of oligo depleting potentials for all organs show very high agreement within most organs, as shown in Supplementary Figure 4-12. This is not the case, however, when organs from different RNase digestion groups are compared. In these cases, correlation coefficients are between 0.14 and 0.64 (mean value of 0.28). This observation suggests that oligos designed for an experiment with one RNase are not necessarily transferable to an experiment with a different RNase.

Furthermore, if the same RNase digestion protocol is used, oligos designed for one tissue (assuming only high potential oligos are selected) do not necessarily provide efficient depletion in another. In some cases, the oligos with high depleting potential in one tissue show high depleting potential in others (kidney-*vs*-skeletal muscle, for example), however, this is only the case for a minority of tissues. Most tissue pairs show a low correlation in rRNA depleting potential of oligos. For example, pancreas-*vs*-heart and skeletal muscle-*vs*-lung both have Pearson’s correlation coefficients of below 0.25, demonstrating that some oligos are very tissue-specific, with low transferability to other tissues. These observations agree with our data analyzing positional abundance profiles, as presented in the previous section.



### 3.4 Improving overall rRNA depletion efficiency using *Ribo-ODDR*, *in vivo* oligo design example

To demonstrate the conveniency and power of using *Ribo-ODDR*, we performed two groups of *in vivo* Ribo-seq experiments in mouse intestine, using the same experimental protocol with the exception of the rRNA depletion oligos used (see Figure 6).

Prior to this experiment, we performed two *in vitro* experiments in order to create a preliminary set of mouse rRNA depletion oligos. To do this, we adopted the Ribo-seq protocol from a previously published study focusing on human cell lines [21], and performed our experiments with mouse intestinal organoids using human rRNA depletion oligos (SET-0, Supplementary Table 1). In our analysis of this experiment, we observed that ~87% of the reads that mapped to rRNAs and protein-coding transcripts were rRNA fragments. Additionally, we could detect rRNA fragments originating from regions of the mouse rRNA that were targeted by the human depletion oligos (see Supplementary Figure 13).

To improve the overall quality of our Ribo-seq experiments, we used the early versions of *Ribo-ODDR cross-species optimization mode* to optimize these human oligos (SET-0) for mouse experiments, and added four new oligos to the pool by manually visualizing rRNA fragments and selecting the hotspots requiring depletion. While this approach did result in increased depletion of rRNAs *in vitro*, the effect was minor, with this new set of oligos (SET-1) averaging ~17% protein-coding transcript mapping reads, compared to ~13% with SET-0 oligos. The sequences of the SET-1 oligos are given in Supplementary Table 2.

Using these SET-1 oligos, we carried out an *in vivo* experiment and generated pilot data to repeat the process. Based on this data, we used *Ribo-ODDR* to design an additional 5 oligos with a high potential rRNA depletion and added them to creating SET-2 (see Supplementary Table 3). In Figure 7 and Supplementary Figure 14, we show that positional abundance profile of rRNA fragments are highly conserved between replicates in each experiment group, and newly designed oligos in SET-2 were successful at depleting the fragments in their corresponding regions. Crucially, rRNA depletion was more efficient after the addition of five *Ribo-ODDR* designed oligos, result-

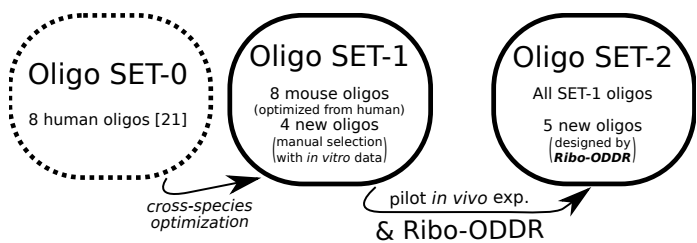


Figure 6: Oligo sets used in this paper. SET-1 consists of mouse-optimized version of eight SET-0 oligos and four additional ones, manually selected based on pilot *in vitro* experiments. SET-2 includes all SET-1 oligos and 5 new oligos, designed by *Ribo-ODDR* with data from pilot *in vivo* experiments using SET-1 oligos for rRNA depletion.

ing in a ~5-fold increase in protein-coding transcript reads (~27% vs ~5%), with SET-2 oligos giving ~72% rRNA fragments on average, compared to ~94% rRNA fragments on average for experiments using SET-1 oligos. This substantial increase in rRNA depletion efficiency demonstrates the power of experiment-specific rRNA depletion in Ribo-seq experiments and how using *Ribo-ODDR* can help this process.

## 4 DISCUSSION

Ribosome profiling has become a mainstay experiment in the analysis of RNA translation. It is the most informative technique available for studying the translatome and has become very widely used in the decade since its development [1]. However, as the technique focuses on ribosomally bound RNAs, the enrichment of rRNAs is an unfortunate necessity of the protocol. The nuclease cleavage of these rRNA produces fragments of a similar size to those being analyzed, creating an obvious technical challenge. Indeed, rRNA fragments commonly far outnumber reads from protein coding genes. As a result, rRNA depletion is a vital step in generating high quality Ribo-seq data.

The most common approach to overcome this issue is the use of commercially available rRNA depletion kits. However, our data shows that the efficiency of depletion using this method is variable, and suggests that combining this method with a small number of custom designed oligos could significantly increase rRNA depletion. Additionally, previously published studies

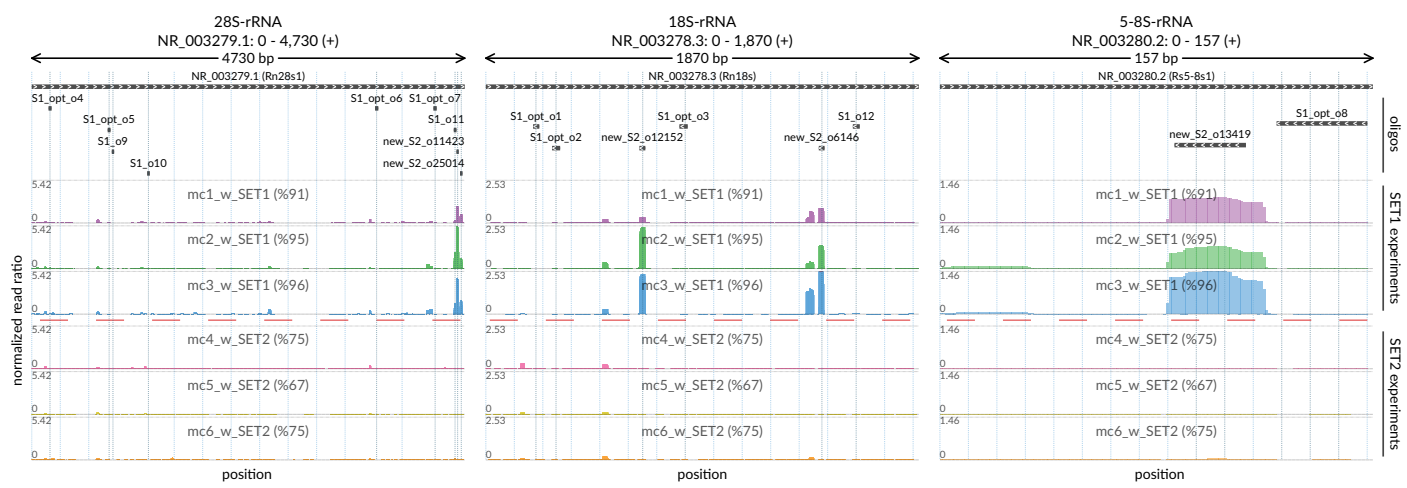


Figure 7: Positional abundance profiles of 28S (left), 18S (middle) and 5-8S (right) rRNA fragments coming from *in vivo* (mouse intestine) Ribo-seq experiments performed with two different sets of rRNA depletion oligos, SET-1 and SET-2. The latter set includes all oligos from the former and 5 additional oligos designed with *Ribo-ODDR*, based on pilot data generated using only SET-1 oligos. In each figure, top track indicates the target regions of used oligos within that rRNA, where additional oligos of the SET-2 are labeled as ‘new’. In all tracks, x-axis corresponds to position within rRNAs. In profile tracks, y-axis is fixed for all samples and shows the normalized read ratio, number of rRNA reads mapped to the position divided by the total number of reads mapped to all protein coding transcripts. The percentages given within sample labels indicates the sample-specific percentage of rRNA fragments, within all reads that is mapped to rRNAs and protein-coding transcripts.

have suggested that the use of commercial kits can result in bias in individual mRNA fragments [8], emphasising that the rRNA depletion strategy must be considered when planning experiments.

Using publically available data, we have also shown that this issue is compounded by variability in the specific rRNA fragments that is introduced by differing experimental conditions. Both the origin of the tissue, and the nuclease used for RNA digestion significantly change the rRNA fragment population, showing that a depletion strategy that works for one experiment will not necessarily work in another situation. The source of the tissue-specific rRNA fragment heterogeneity is unknown, however it may be due to differences in the accessibility to the tissue of the nuclease. Ultimately, significant sequencing depth can be gained by improving the rRNA depletion. This may be particularly important in samples and tissues that have previously proven difficult to assay using Ribo-seq, such as the intestinal epithelium and other *in vivo* tissues.

We developed *Ribo-ODDR* to aid with the design of

oligos in an experiment by experiment manner. The tool enables users to run the *design mode* for multiple optimization rounds until the desired rRNA depletion is reached. After each round of profiling, a number of user-selected high depletion potential oligos can be added, increasing the efficiency of depletion of subsequent experiments until the desired protein coding sequencing depth is reached. It is important to note that *Ribo-ODDR* does not take into account what depletion strategy is already being used and still computes the depleting potential of depletion oligos that are already included in the protocol. As a result, *Ribo-ODDR* can only be used to increase the efficiency of depletion by adding oligos to the previously used rRNA depletion protocol. However, we have shown that using such an iterative approach can increase the percentage of protein coding transcripts detected 5-fold, turning a failed experiment into a successful one.

An obvious drawback of this approach is the need for preliminary data to optimize the depletion strategy. In order to optimally carry out a Ribo-seq experiment,

it is advisable to generate such preliminary data using the exact protocol as planned under experimental conditions, particularly when using tissues that have previously proven difficult to work with. However, as a result of the increasing number of Ribo-seq studies being published, in many cases it may be sufficient to use data from a similar source tissue that has previously published. This could then be analysed using *Ribo-ODDR* to create an oligo set that is likely to efficiently deplete rRNA.

Alternative depletion strategies have also been suggested, such as the use of duplex-specific nuclease (DSN) [8], which we have not compared to *Ribo-ODDR*-based depletion. However, it is important to point out that *Ribo-ODDR* is not necessarily a stand-alone method. We envision that *Ribo-ODDR* will be used alone in some cases, and in conjunction with other depletion strategies in others. For instance, we have shown that commercial kits can benefit from the addition of a small number of custom designed oligos.

*Ribo-ODDR* gives experimenters a platform to assess the most optimal oligos, allowing for increased depth of mRNA fragment sequencing, and maximizing the information gained in Ribo-seq experiments.

## 5 CONCLUSION

In this study, we show that the use of commercial kits may result in suboptimal rRNA depletion in Ribo-seq experiments, and that different tissues and experimental conditions result in heterogeneity of produced rRNA fragments. Both of these findings demonstrate the necessity of experiment-specific oligo design for efficient rRNA depletion. To aid the computational part of oligo design process, we have developed *Ribo-ODDR*, a Ribo-seq focused oligo design pipeline for experiment-specific rRNA depletion. Oligos designed using this platform resulted in a substantial increase in rRNA depletion *in vivo* Ribo-seq experiments in mouse intestine. The tool is easy to use, and will allow the optimization of this crucial step in the Ribo-seq protocol, particularly for samples that have proven difficult to assay.

*Ribo-ODDR* is an open source software and freely accessible at <https://github.com/fallerlab/Ribo-ODDR>.

## 6 ACKNOWLEDGEMENTS

We would like to thank other members of the Faller Lab and Abhijeet Pataskar for critical reading and fruitful discussions.

## 7 FUNDING

This work was funded by the Dutch Cancer Society (KWF Kankerbestrijding) Project [NKI-2016-10535]. JS is funded by an EMBO Long Term Fellowship [210-2018].

## 8 Supplementary Figures and Tables

- **Supplementary Figure 1:** Screenshot from the oligo selection user interface, *Ribo-ODDR oligo-selector*.
- **Supplementary Figure 2:** Positional abundance profile of 5-8S and 5S rRNA fragments generated by three Ribo-seq experiments despite using the Ribo-Zero kit.
- **Supplementary Figure 3:** Tissue and RNase specificity of rRNA fragments in mouse, based on positional abundance profile of 18S, 5-8S and 5S rRNA fragments.
- **Supplementary Figure 4:** Sample-specificity of rRNA fragments and cross-replicate correlation analysis of oligo depleting potentials for brain.
- **Supplementary Figure 5:** Sample-specificity of rRNA fragments and cross-replicate correlation analysis of oligo depleting potentials for heart.
- **Supplementary Figure 6:** Sample-specificity of rRNA fragments and cross-replicate correlation analysis of oligo depleting potentials for kidney.
- **Supplementary Figure 7:** Sample-specificity of rRNA fragments and cross-replicate correlation analysis of oligo depleting potentials for liver.
- **Supplementary Figure 8:** Sample-specificity of rRNA fragments and cross-replicate correlation analysis of oligo depleting potentials for skeletal muscle.

- **Supplementary Figure 9:** Sample-specificity of rRNA fragments and cross-replicate correlation analysis of oligo depleting potentials for testis.
- **Supplementary Figure 10:** Sample-specificity of rRNA fragments and cross-replicate correlation analysis of oligo depleting potentials for lung.
- **Supplementary Figure 11:** Sample-specificity of rRNA fragments and cross-replicate correlation analysis of oligo depleting potentials for pancreas.
- **Supplementary Figure 12:** Sample-specificity of rRNA fragments and cross-replicate correlation analysis of oligo depleting potentials for spleen.
- **Supplementary Figure 13:** Positional abundance profiles of rRNA fragments coming from *in vitro* Ribo-seq experiments.
- **Supplementary Figure 14:** Alternative visualisation for positional abundance profiles of rRNA fragments coming from *in vivo* Ribo-seq experiments.
- **Supplementary Table 1:** Size selection marker, adapter and primer sequences.
- **Supplementary Table 2:** Sequences for SET-0 oligos.
- **Supplementary Table 3:** Sequences for SET-1 oligos.
- **Supplementary Table 4:** Sequences for SET-2 oligos.

#### 8.0.1 Conflict of interest statement.

None declared.

## References

- [1] N. T. Ingolia, S. Ghaemmaghami, J. R. Newman, and J. S. Weissman. Genome-wide analysis *in vivo* of translation with nucleotide resolution using ribosome profiling. *Science*, 324(5924):218–223, Apr 2009.
- [2] Y. Wang, H. Zhang, and J. Lu. Recent advances in ribosome profiling for deciphering translational regulation. *Methods*, May 2019.
- [3] W. R. Blevins, T. Tavella, S. G. Moro, B. Blasco-  
Moreno, A. Closa-Mosquera, J. Diez, L. B. Carey,  
and M. M. Alba. Extensive post-transcriptional buffering of gene expression in the response to severe oxidative stress in baker’s yeast. *Sci Rep*, 9(1):11005, Jul 2019.
- [4] N. J. McGlincy and N. T. Ingolia. Transcriptome-wide measurement of translation by ribosome profiling. *Methods*, 126:112–129, 08 2017.
- [5] M. V. Gerashchenko and V. N. Gladyshev. Ribonuclease selection for ribosome profiling. *Nucleic Acids Res.*, 45(2):e6, 01 2017.
- [6] B. Liu, G. Molinaro, H. Shu, E. E. Stackpole, K. M. Huber, and J. D. Richter. Optimization of ribosome profiling using low-input brain tissue from fragile X syndrome model mice. *Nucleic Acids Res.*, 47(5):e25, 03 2019.
- [7] M. V. Gerashchenko, A. V. Lobanov, and V. N. Gladyshev. Genome-wide ribosome profiling reveals complex translational regulation in response to oxidative stress. *Proc. Natl. Acad. Sci. U.S.A.*, 109(43):17394–17399, Oct 2012.
- [8] B. Y. Chung, T. J. Hardcastle, J. D. Jones, N. Irigoyen, A. E. Firth, D. C. Baulcombe, and I. Brierley. The use of duplex-specific nuclease in ribosome profiling and a user-friendly software package for Ribo-seq data analysis. *RNA*, 21(10):1731–1745, Oct 2015.
- [9] A. J. Kraus, B. G. Brink, and T. N. Siegel. Efficient and specific oligo-based depletion of rRNA. *Sci Rep*, 9(1):12281, Aug 2019.
- [10] D. Simsek, G. C. Tiu, R. A. Flynn, G. W. Byeon, K. Leppek, A. F. Xu, H. Y. Chang, and M. Barna. The Mammalian Ribo-interactome Reveals Ribosome Functional Diversity and Heterogeneity. *Cell*, 169(6):1051–1065, Jun 2017.
- [11] Marcel Martin. Cutadapt removes adapter sequences from high-throughput sequencing reads. *EMBnet.journal*, 17(1):10–12, 2011.
- [12] D. Kim, G. Pertea, C. Trapnell, H. Pimentel, R. Kelley, and S. L. Salzberg. TopHat2: accurate alignment of transcriptomes in the presence of insertions, deletions and gene fusions. *Genome Biol.*, 14(4):R36, Apr 2013.

[13] E. Kopylova, L. Noe, and H. Touzet. Sort-MeRNA: fast and accurate filtering of ribosomal RNAs in metatranscriptomic data. *Bioinformatics*, 28(24):3211–3217, Dec 2012.

[14] Maxim V. Gerashchenko, Zalan Peterfi, and Vadim N. Gladyshev. Organ-specific translation elongation rates measured by in vivo ribosome profiling. *bioRxiv*, 2018.

[15] F. Alkan, A. Wenzel, O. Palasca, P. Kerpedjiev, A. F. Rudebeck, P. F. Stadler, I. L. Hofacker, and J. Gorodkin. RIsearch2: suffix array-based large-scale prediction of RNA-RNA interactions and siRNA off-targets. *Nucleic Acids Res.*, 45(8):e60, 05 2017.

[16] R. Lorenz, S. H. Bernhart, C. Honer Zu Siederdissen, H. Tafer, C. Flamm, P. F. Stadler, and I. L. Hofacker. ViennaRNA Package 2.0. *Algorithms Mol Biol*, 6:26, Nov 2011.

[17] N. Barker, J. H. van Es, J. Kuipers, P. Kujala, M. van den Born, M. Cozijnsen, A. Haegebarth, J. Korving, H. Begthel, P. J. Peters, and H. Clevers. Identification of stem cells in small intestine and colon by marker gene Lgr5. *Nature*, 449(7165):1003–1007, Oct 2007.

[18] F. el Marjou, K. P. Janssen, B. H. Chang, M. Li, V. Hindie, L. Chan, D. Louvard, P. Chambon, D. Metzger, and S. Robine. Tissue-specific and inducible Cre-mediated recombination in the gut epithelium. *Genesis*, 39(3):186–193, Jul 2004.

[19] E. Sanz, L. Yang, T. Su, D. R. Morris, G. S. McKnight, and P. S. Amieux. Cell-type-specific isolation of ribosome-associated mRNA from complex tissues. *Proc. Natl. Acad. Sci. U.S.A.*, 106(33):13939–13944, Aug 2009.

[20] W. J. Faller, T. J. Jackson, J. R. Knight, R. A. Ridgway, T. Jamieson, S. A. Karim, C. Jones, S. Radulescu, D. J. Huels, K. B. Myant, K. M. Dudek, H. A. Casey, A. Scopelliti, J. B. Cordero, M. Vidal, M. Pende, A. G. Ryazanov, N. Sonnenberg, O. Meyuhas, M. N. Hall, M. Bushell, A. E. Willis, and O. J. Sansom. mTORC1-mediated translational elongation limits intestinal tumour initiation and growth. *Nature*, 517(7535):497–500, Jan 2015.

[21] F. Loayza-Puch, J. Drost, K. Rooijers, R. Lopes, R. Elkon, and R. Agami. p53 induces transcriptional and translational programs to suppress cell proliferation and growth. *Genome Biol.*, 14(4):R32, Apr 2013.

[22] A. A. Egorov, E. A. Sakharova, A. S. Anisimova, S. E. Dmitriev, V. N. Gladyshev, and I. V. Kulakovskiy. svist4get: a simple visualization tool for genomic tracks from sequencing experiments. *BMC Bioinformatics*, 20(1):113, Mar 2019.